RESEARCH ARTICLE
PLANETARY SCIENCES

Earth and Planetary Physics
4: 543–549, 2020
doi: 10.26464/epp2020064

Solar control of CO_2^+ ultraviolet doublet emission on Mars

ZiChuan Li[1,2], Jun Cui[3,4*], Jing Li[3], XiaoShu Wu[1,4], JiaHao Zhong[3], and FaYu Jiang[5]

[1]National Astronomical Observatories, Chinese Academy of Sciences, Beijing 100012, China;

[2]School of Astronomy and Space Sciences, University of Chinese Academy of Sciences, Beijing 100049, China;

[3]Planetary Environmental and Astrobiological Research Laboratory (PEARL), School of Atmospheric Sciences, Sun Yat-Sen University, Zhuhai Guangdong 519082, China;

[4]Center for Excellence in Comparative Planetology, Chinese Academy of Sciences, Hefei 230026, China;

[5]Lunar and Planetary Laboratory, University of Arizona, Tucson, Arizona, USA

Key Points:

- The brightness profiles of CO_2^+ UVD emission on Mars were obtained from the MAVEN IUVS limb observations
- Strong solar cycle and solar zenith angle variations in peak emission intensity and altitude were revealed by the data
- An extra driver, presumably related to the complicated variation in the background atmosphere, is required to fully interpret the observations

Citation: Li, Z. C., Cui, J., Li, J., Wu, X. S., Zhong, J. H. and Jiang, F. Y. (2020). Solar control of CO_2^+ ultraviolet doublet emission on Mars. *Earth Planet. Phys.*, *4*(6), 543–549. http://doi.org/10.26464/epp2020064

Abstract: The CO_2^+ ultraviolet doublet (UVD) emission near 289 nm is an important feature of dayside airglow emission from planetary upper atmospheres. In this study, we analyzed the brightness profiles of CO_2^+ UVD emission on Mars by using the extensive observations made by the Imaging Ultraviolet Spectrograph on board the recent Mars Atmosphere and Volatile Evolution spacecraft. Strong solar cycle and solar zenith angle variations in peak emission intensity and altitude were revealed by the data: (1) Both the peak intensity and altitude increase with increasing solar activity, and (2) the peak intensity decreases, whereas the peak altitude increases, with increasing solar zenith angle. These observations can be favorably interpreted by the solar-driven scenario combined with the fact that photoionization and photoelectron impact ionization are the two most important processes responsible for the production of excited-state CO_2^+ and consequently the intensity of CO_2^+ UVD emission. Despite this, we propose that an extra driver, presumably related to the complicated variation in the background atmosphere, such as the occurrence of global dust storms, is required to fully interpret the observations. In general, our analysis suggests that the CO_2^+ UVD emission is a useful diagnostic of the variability of the dayside Martian atmosphere under the influences of both internal and external drivers.

Keywords: Mars; dayglow; CO_2^+; MAVEN

1. Introduction

Airglow emission provides important information on the energy deposition in and chemistry of a planetary upper atmosphere (Slanger et al., 2008, and references therein). For Mars, a typical dayglow spectrum in the ultraviolet (UV) region includes the CO Cameron band, the CO fourth positive band, the CO_2^+ ultraviolet doublet (UVD), the CO_2^+ Fox–Duffendack–Barker band, and several distinctive emission lines from atomic C, O, and H (Barth et al., 1971; Stewart, 1972; Stewart et al., 1972). More recently, additional faint emission features, such as the N_2 Vegard–Kaplan band, the NO γ band, and the CO^+ first negative band, have been identified (Leblanc et al., 2006; Jain et al., 2015; Stevens et al., 2015, 2019). Existing analyses suggest that these dayglow emission features are mostly produced by either photon or photoelectron impact excitation (Fox and Dalgarno, 1979; Fox, 1992).

Among the important emission features of a Martian dayglow spectrum, the CO_2^+ UVD ($B^2\Sigma_u^+ - X^2\prod_g$) emission near 289 nm has captured extensive research interest over the past several decades. Since 1969, the CO_2^+ UVD emission on Mars has been measured remotely by the UV spectrometer or spectrograph on board Mariner 6, 7, and 9 (Barth et al., 1969, 1971; Stewart, 1972; Stewart et al., 1972), the Spectroscopy for Investigation of Characteristics of the Atmosphere of Mars (SPICAM) on board the Mars Express (MEx; Leblanc et al., 2006), and the Imaging Ultraviolet Spectrograph (IUVS) on board the Mars Atmosphere and Volatile Evolution (MAVEN; Jain et al., 2015). This feature is mainly caused by the photoionization and photoelectron impact ionization of CO_2, which produces excited-state CO_2^+ (Fox and Dalgarno, 1979; Cox et al., 2010; Gérard et al., 2019). Fluorescent scattering of solar photons also contributes but is usually negligible at altitudes below 180 km (Fox and Dalgarno, 1979).

Correspondence to: J. Cui, cuijun7@mail.sysu.edu.cn
Received 10 JUN 2020; Accepted 28 JUL 2020.
Accepted article online 07 AUG 2020.

Previous analyses of CO_2^+ UVD emission have mainly focused on the observed brightness profiles and their variations. The average peak brightness measured by the MEx SPICAM (Leblanc et al., 2006) is ~30 kR (kilorayleigh) for the solar zenith angle (SZA) range from 30° to 60°. With the aid of the more recent MAVEN IUVS measurements, Jain et al. (2015) reported a peak brightness of ~76 kR over a similar SZA range. The difference in peak intensity between the two works is mainly attributable to the solar cycle variation. The former is appropriate for a moderate solar activity condition with a solar radio index at 10.7 cm, denoted as $F_{10.7}$, of 105 in solar flux units (SFU, 10^{-22} $Wm^{-2}Hz^{-1}$), and the latter is appropriate for a higher solar activity condition, with $F_{10.7}$ of ~160 SFU. Regarding the peak altitude of CO_2^+ UVD emission, the MEx SPICAM observations indicate that it is typically at 120–130 km and increases with increasing SZA (Leblanc et al., 2006). However, the SZA trend in peak altitude has not been confirmed by the MAVEN IUVS observations (Jain et al., 2015).

The MAVEN spacecraft has been orbiting Mars since September 2014 (Jakosky et al., 2015), operating with a better trajectory design around the planet in terms of UV observations as compared with the MEx. It has an elliptical trajectory in a 4.5-hr orbit with an inclination of 75°. The apoapsis altitude is ~6,200 km and the periapsis altitude is 150–160 km during the nominal mission phase but could be as low as 120–130 km during isolated "deep-dip" campaigns. The MAVEN IUVS instrument has collected thousands of CO_2^+ UVD emission profiles in different Mars seasons and under different solar activity conditions, providing a more extensive data set complementary to the earlier Mariner and MEx observations. Furthermore, the Extreme Ultraviolet Monitor (EUVM) on board MAVEN is able to make simultaneous measurements of short-wave solar irradiance received directly at Mars, allowing a better understanding of the solar control of CO_2^+ UVD emission.

The present study is aimed at a systematic investigation of CO_2^+ UVD emission on Mars by using the MAVEN IUVS measurements. We describe in Section 2 the data set used. In Section 3, we present the observed solar cycle and SZA variations in both peak emission altitude and intensity. This is followed by possible interpretations in Section 4 and concluding remarks in Section 5.

2. MAVEN Imaging Ultraviolet Spectrograph Observations

The IUVS is one of the eight scientific instruments on board the MAVEN spacecraft, measuring the far UV airglow on Mars between 110 and 190 nm at ~0.6 nm resolution and the middle UV airglow between 180 and 340 nm at ~1.2 nm resolution (McClintock et al., 2015). The IUVS is mounted on an articulated payload platform, which directs the orientation of the instrument slit as it captures the spectra of the Martian atmosphere. The IUVS has three operational modes, limb scan, coronal scan, and disk scan, whose implementation depends on the orbital phase. Here we consider limb observations that cover the tangent point altitude range of 80–225 km. Limb scans are taken near the periapsis, with the slit orientation parallel to the surface. A scan mirror sweeps the slit up and down, allowing the IUVS to perform periapsis observations at different altitudes with ~5 km resolution. A maximum number of 12 limb scans are taken during a single orbit. The observed raw data counts are corrected for detector dark currents and then converted to physical brightness by using the sensitivity derived from UV bright stellar observations made during the MAVEN cruise phase. The middle UV and far UV systematic uncertainties estimated from stellar calibrations are 30% and 25%, respectively.

The IUVS instrument team provides three levels of data product on the National Aeronautics and Space Administration Planetary Data System: level 1A (raw data), level 1B (calibrated data), and level 1C (processed data). The processed data provide the brightness profiles for a total number of 28 individual emission lines, which are obtained through multiple linear regression fits of individual spectral components combined with the laboratory spectral data and the reflected solar spectrum background (Stevens et al., 2015). In this study, we used the level 1C data files, which are tagged "periapse" with version tag V13_R01.

We include in this study 2,189 MAVEN orbits that cover the time period from March 2015, reflecting southern summer conditions in Martian year (MY) 32, to October 2018, also reflecting southern summer conditions but in MY 34. The IUVS limb scan observations are available during each of these orbits, providing a suffi-

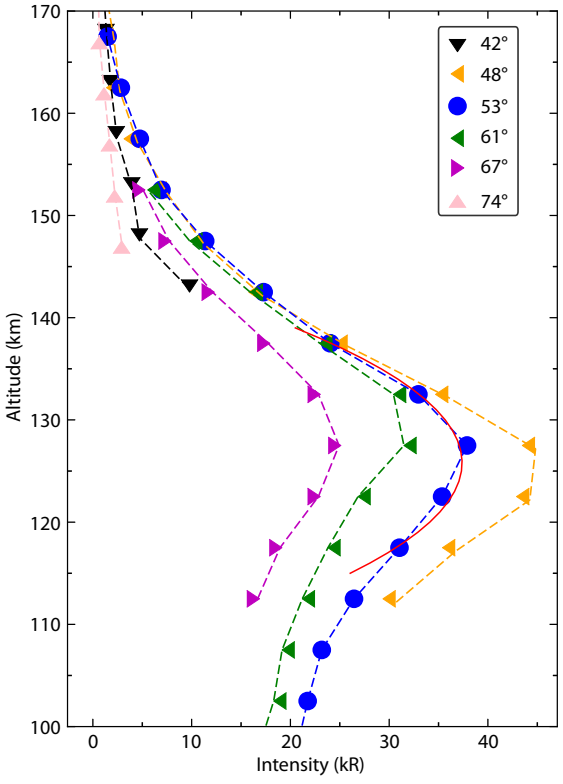

Figure 1. Several representative CO_2^+ ultraviolet doublet brightness profiles obtained with the imaging ultraviolet spectrograph limb observations during MAVEN orbit number 2,938 on 3 April 2016 over the altitude range of 100–170 km. The profile closest to the median situation is marked by blue, and the second-order polynomial fitting to the observations within 20 km centered at the apparent emission peak is indicated by red. The solar zenith angle for each brightness profile is also indicated in the figure legend for reference.

ciently large sample to analyze the variations in CO_2^+ UVD emission on Mars. For each orbit, we computed the respective median brightness profile with the criterion that at least 10 individual measurements have been recorded over the altitude range of 100–170 km and restricted to SZA below 75°. Several representative CO_2^+ UVD brightness profiles are presented in Figure 1, obtained during MAVEN orbit number 2,983 appropriate for SZA ~53°. The profile closest to the median situation is indicated by the blue line. Individual brightness profiles, whenever with tangent points penetrating down to sufficiently low altitudes, show peak emission at 120–130 km. Analogous to Gkouvelis et al. (2018), the peak altitude and intensity were estimated from the second-order polynomial fitting to individual measurements made within ~20 km centered at the apparent emission peak, as indicated by the red line in Figure 1. A similar procedure was applied to the entire data set. The typical uncertainty in peak altitude is ~1 km and the typical uncertainty in peak intensity is less than 5%, both small enough to allow their variations in the Martian upper atmosphere to be retrieved.

Figure 2 shows the distribution of the MAVEN IUVS observations used in this study, in terms of the SZA and integrated solar extreme ultraviolet (EUV) and X-ray flux. The SZA refers to the peak of the median brightness profile obtained for each orbit. For the integrated solar flux as a proxy of solar activity, we used the level 3 solar spectral model constructed from the Flare Irradiance Spectral Model–Mars (version 11) and calibrated it with the MAVEN EUVM band irradiance data (Eparvier et al., 2015; Thiemann et al., 2017). The integration was made over the wavelength range of 0.5–69 nm, where 69 nm corresponds to the minimum photon energy required to produce excited-state CO_2^+.

3. Variations in CO_2^+ Ultraviolet Doublet Emission

For the MAVEN IUVS data set analyzed in this study, the mean peak intensity of CO_2^+ UVD emission is 38 kR with a scattering of ~34%, where the scattering is defined as the standard deviation in peak intensity divided by the median peak intensity. The maximum peak intensity is 95 kR in MY 32 and the minimum intensity is 12 kR in MY 34. The mean peak altitude is at 120 km with a scattering of ~7%. The highest and lowest peak altitudes are 146 km in MY 33 and 107 km in MY 34, respectively. These values suggest the presence of strong variations in the peak parameters of CO_2^+ UVD emission, which we detail below.

3.1 Variations in the CO_2^+ Ultraviolet Doublet Peak Intensity

The SZA variations in the median peak intensity of CO_2^+ UVD emission are presented in Figure 3, distinguishing between different solar activity conditions characterized by different ranges of the integrated solar flux over 0.5–69 nm. The vertical and horizontal bars indicate the standard deviations of peak intensity and SZA within each bin. Each bin contains at least 10 individual brightness profiles to ensure that the derived SZA variations are statistically robust. The figure demonstrates a clear trend of decreasing peak intensity with increasing SZA at all solar activity conditions. The observed dependence of the peak intensity on SZA could be reasonably described by a cosine function in the form of

$$I = I_{sub}\cos(\mathrm{SZA}), \quad (1)$$

where I_{sub} is the subsolar peak intensity. The best-fit cosine functions are indicated by the dashed lines in Figure 3, predicting a subsolar peak intensity of 56 kR, 71 kR, and 102 kR, respectively, for the integrated solar flux below 0.9 mW·m^{-2}, between 0.9 and 1.3 mW·m^{-2}, and above 1.3 mW·m^{-2}.

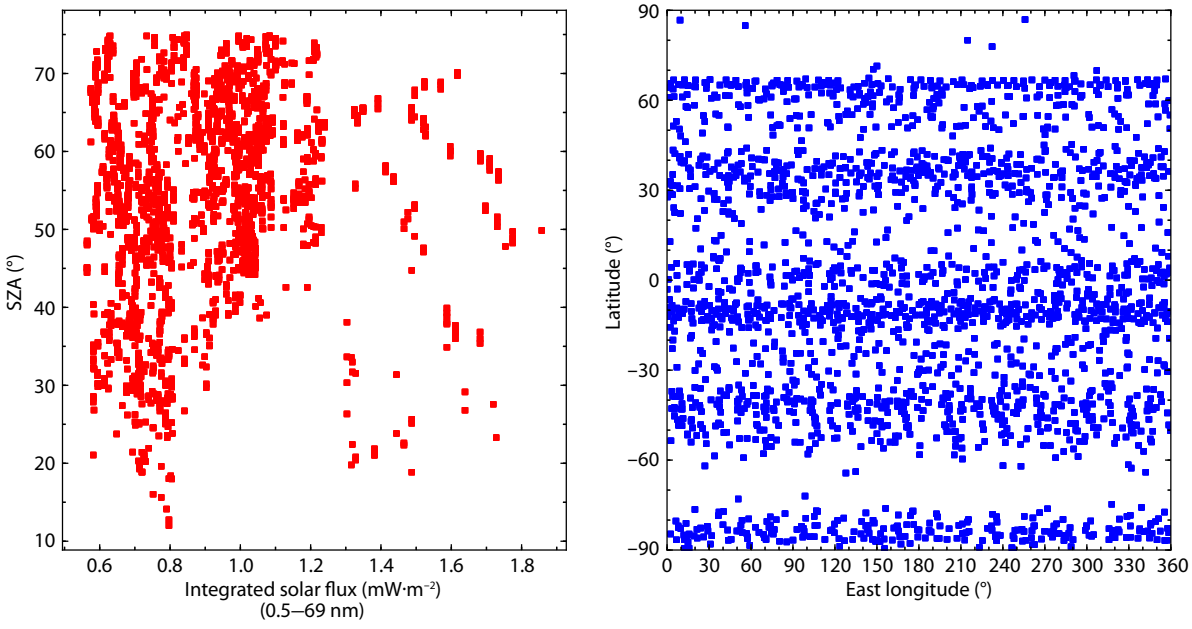

Figure 2. Distribution of the MAVEN imaging ultraviolet spectrograph observations used in the present study, in terms of the solar zenith angle (SZA) and integrated solar flux at 0.5–69 nm (left) and in terms of the longitude and latitude (right). The SZA, longitude, and latitude refer to the peak of the median brightness profile during each orbit, whereas the integrated solar flux is computed based on the level 3 solar spectral model at Mars constructed from the MAVEN Extreme Ultraviolet Monitor band irradiance data.

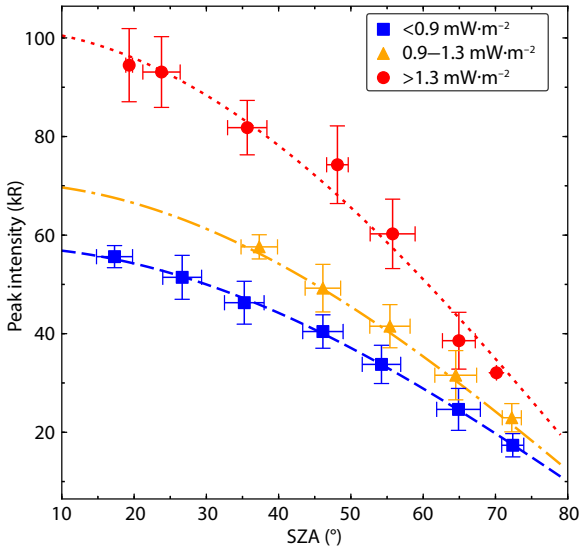

Figure 3. The median peak intensity of CO_2^+ ultraviolet doublet emission as a function of the solar zenith angle (SZA) for different ranges of the integrated solar flux (0.5–69 nm), as indicated in the figure legend. The vertical and horizontal bars represent the standard deviations of peak intensity and SZA within each bin. The dashed lines show the best-fit cosine functions (see Equation (1)) under different solar activity conditions.

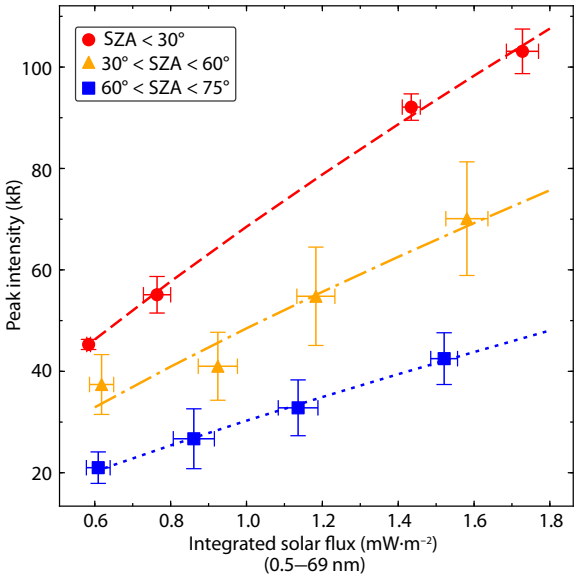

Figure 4. The median peak intensity of CO_2^+ ultraviolet doublet emission as a function of the integrated solar flux (0.5–69 nm) for different solar zenith angle (SZA) ranges, as indicated in the figure legend. The vertical and horizontal bars represent the standard deviations of peak intensity and solar flux within each bin. The dashed lines show the best-fit power law relations (see Equation (2))at different SZA ranges.

A comparison of the subsolar intensities quoted above demonstrates the presence of strong solar cycle variation, which is further displayed in Figure 4 by using the integrated solar flux over 0.5–69 nm as a proxy of solar activity. Different SZA ranges are shown separately: red for 0°–30°, blue for 30°–60°, and green for 60°–75°, respectively. The vertical and horizontal bars represent the standard deviations of peak intensity and solar flux within each bin. Each bin contains at least 18 individual brightness profiles to ensure that the derived solar cycle variations are statistically robust. The figure reveals a remarkable increase in peak intensity with increasing solar activity, which is persistent at all SZAs. Here we use the power law relation to describe the solar cycle variation in peak intensity, hereafter denoted as I, which is written as

$$I = \tilde{I}\left(F_{69\mathrm{nm}}/\tilde{F}_{69\mathrm{nm}}\right)^{\alpha}, \tag{2}$$

where $F_{69\mathrm{nm}}$ is the integrated solar flux over 0.5–69 nm, $\tilde{I}$ is the peak intensity at a reference solar flux of $\tilde{F}_{69\mathrm{nm}}$ chosen to be 1 mW·m^{-2}, and α is the power index to be constrained by the data. Such a power law relation is chosen to properly reflect the expected limiting behavior of zero peak intensity when the solar radiation is switched off. The best-fit relations are given by the dashed lines in the figure, demonstrating a comparable solar cycle variation with a common power index of ~0.77 independent of the SZA. The best-fit peak intensity for a reference solar flux of 1 mW·m^{-2} is 69 kR at SZA < 30°, 48 kR at 30° < SZA < 60°, and 30 kR at 60° < SZA < 75°, respectively, suggesting a trend that is compatible with the SZA variation displayed in Figure 3.

3.2 Variations in the CO_2^+ Ultraviolet Doublet Peak Altitude

This section is devoted to the solar control of the peak altitude of CO_2^+ UVD emission. We show in Figure 5 the median peak altitude of CO_2^+ UVD emission as a function of the SZA, obtained for different ranges of the integrated solar flux over 0.5–69 nm. The horizontal and vertical bars in the figure show the standard deviations of peak altitude and SZA in each bin. The figure reveals a nearly constant peak altitude at SZA < 40°, accompanied by an appreciable increase with increasing SZA toward the terminator. Analogous to the SZA variation in peak electron altitude in the dayside Martian ionosphere (e.g., Morgan et al., 2008; Fox and Weber, 2012; Yao MJ et al., 2019), the SZA variation in the peak emission altitude can be approximately described by a logarithmic secant relation in the form of

$$Z = Z_{\mathrm{sub}} + H \times \ln\left[\sec\left(\mathrm{SZA}\right)\right], \tag{3}$$

where Z_{sub} denotes the subsolar peak altitude in kilometers and H is a length scale to be constrained by the data. The best-fit subsolar peak altitudes are 115 km, 120 km, and 122 km, respectively, for the solar flux range of below 0.9 mW·m^{-2}, between 0.9 and 1.3 mW·m^{-2}, and above 1.3 mW·m^{-2}. The length scale, H, is estimated to be 6.5 km, 7.0 km, and 5.5 km, respectively, under these solar cycle conditions, suggesting that the SZA variation in the peak altitude tends to be less pronounced at high solar activity conditions.

We further show the observed solar cycle variation in peak altitude in Figure 6 where the integrated solar flux over 0.5–190 nm is used as a proxy of solar activity. The IUVS observations made at different SZA ranges are indicated separately in the figure, whereas the vertical and horizontal bars represent the standard deviations of peak altitude and solar flux within each bin. Figure 6 reveals a clear trend of increasing peak altitude with increasing sol-

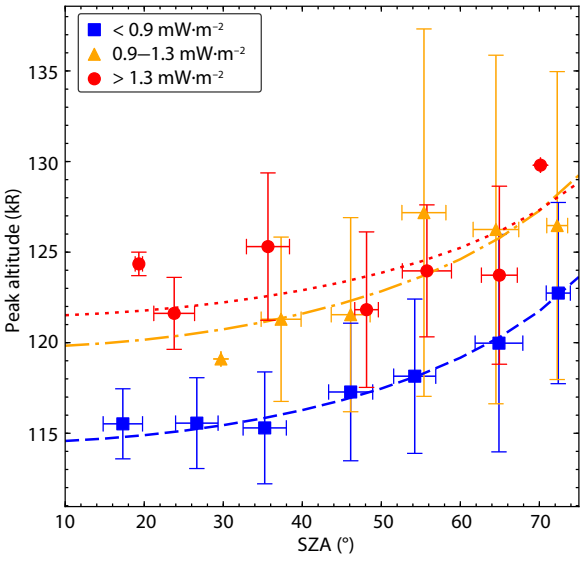

Figure 5. The median peak altitude of CO_2^+ ultraviolet doublet emission as a function of the solar zenith angle (SZA) for different ranges of the integrated solar flux (0.5–69 nm), as indicated in the figure legend. The vertical and horizontal bars represent the standard deviations of peak intensity and SZA within each bin. The dashed lines show the best-fit logarithmic secant relations (see Equation (3)] under different solar activity conditions.

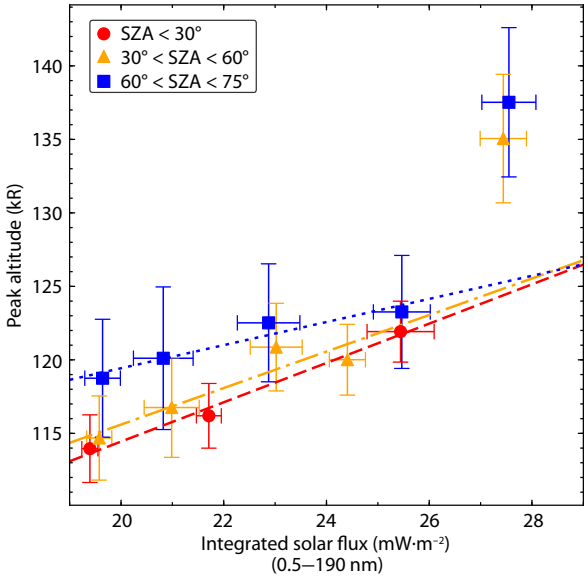

Figure 6. The median peak altitude of CO_2^+ ultraviolet doublet emission as a function of the integrated solar flux (0.5–190 nm) for different solar zenith angle (SZA) ranges, as indicated in the figure legend. The vertical and horizontal bars represent the standard deviations of peak altitude and solar flux within each bin. The dashed lines show the best-fit linear relations (see Equation (4)) obtained for different SZA ranges.

ar flux at all SZAs, which can be empirically modeled with a linear relation in the form of

$$Z = \tilde{Z} + k\left(F_{190\text{nm}}/\tilde{F}_{190\text{nm}}\right), \quad (4)$$

where $\tilde{Z}$ is the peak altitude in kilometers at a reference solar flux of $\tilde{F}_{190\text{nm}}$ chosen to be 10 mW·m^{-2} and k is the linear slope to be constrained by the data. The best-fit reference peak altitude, $\tilde{Z}$, is 101 km, 103 km, and 112 km, respectively, for SZA < 30°, 30° < SZA < 60°, and 60° < SZA < 75°, suggesting a trend that is consistent with the SZA variation depicted in Figure 5. We caution that here we use the solar flux integrated up to 190 nm (instead of 69 nm as before) as a proxy of solar activity, which is closely related to the physical interpretation of the observed variation (see Section 4). Without showing the details, we shall mention that when using $F_{69\text{nm}}$ instead of $F_{190\text{nm}}$ in Figure 6, the correlation between the solar flux and peak altitude is greatly reduced and no unambiguous solar cycle variation could be concluded. Finally, we emphasize that in obtaining the best-fit linear relations, those measurements made with $F_{190\text{nm}}$ > 27 mW·m^{-2} are excluded. This is because under such a condition, the MAVEN IUVS was coincidently observing the Martian upper atmosphere during global dust storms (Fu MH et al., 2020), which would elevate the entire brightness profile, including the emission peak, to higher altitudes (see also Section 4).

4. Interpreting the Variations in CO_2 Ultraviolet Doublet Emission

In Section 3, we reported the solar cycle and SZA variations in both peak intensity and altitude of CO_2^+ UVD emission with the aid of the extensive limb scan observations made by the MAVEN IUVS.

The solar cycle and SZA variations in peak intensity are clearly suggested by the data, showing that the peak intensity increases steadily with increasing solar EUV and X-ray flux and also increases systematically with decreasing SZA. In addition, the same variations in peak altitude are revealed by the data, characterized by an increase in peak altitude with both increasing solar activity and increasing SZA. Different empirical functional forms are adopted to describe the observed variations, as given by Equations (1) –(4).

The observations presented here are favorably compared with those presented in the early IUVS investigation of Jain et al. (2015), who reported a similar correlation between the peak intensity of CO_2^+ UVD emission and the EUVM irradiance measured in the 17–22 nm band (see their Fig. 5), characterized by a linear correlation coefficient of 0.77. The SZA variation in peak altitude was not obtained by Jain et al. (2015), possibly due to the much smaller IUVS sample used in their study. Using the MEx SPICAM observations, Leblanc et al. (2006), however, were able to obtain a similar SZA variation in peak altitude as reported here.

The observations presented so far could be interpreted by the solar-driven scenario in that the variation in peak intensity is a natural result of enhanced photoionization and photoelectron impact ionization under high solar activity conditions, as these are the two processes mainly responsible for the production of excited-state CO_2^+ in the dayside Martian upper atmosphere (e.g., Fox and Dalgarno, 1979). The same scenario also accounts for the observed decrease in peak intensity toward the terminator following a simultaneous decrease in solar irradiance. The above line of reasoning is analogous to the interpretation of the well-known

solar cycle and SZA variations in peak electron density in the dayside Martian ionosphere using the idealized Chapman theory (e.g., Fox and Yeager, 2009). The SZA variation in peak emission altitude could be interpreted by the fact that the emission is peaked where the optical depth at relevant wavelengths reaches unity in the Martian upper atmosphere, also analogous to the interpretation of the established SZA variation in peak electron altitude according to the idealized Chapman theory (e.g., Fox and Weber, 2012). Finally, the solar cycle variation in peak altitude is driven by the expansion of the atmosphere with increasing solar activity, similar to the observed solar cycle variation in exobase altitude at Mars (Fu MH et al., 2020).

Even though the solar-driven scenario successfully interprets the general characteristics of the solar cycle and SZA variations presented so far, we caution that such a simple scenario is not able to account for all the details, as indicated by the considerable scattering of individual IUVS observations, even at a fixed SZA and a fixed solar flux (not shown here). Clearly, an extra driver is required, presumably related to the variation in the background atmosphere, which is far more complicated than the simple effect of atmospheric expansion considered above. Variations driven by thermospheric global circulation (e.g., Bougher et al., 2006, 2009; González-Galindo et al., 2018), wave activity (e.g., England et al., 2017; Siddle et al., 2019), and global dust storms (e.g., Strausberg et al., 2005; Kass et al., 2016; Wu ZP et al., 2020) should all leave noticeable signatures in the observed variations in CO_2^+ UVD emission. In particular, we speculate that the abnormal elevation of the peak emission altitude at the maximum available solar flux, as displayed in Figure 6, is more likely driven by global dust storms rather than thermospheric expansion, but such a speculation needs to be verified by detailed model calculations, which are beyond the scope of the present study.

Existing studies have indeed demonstrated clearly that the brightness profiles of CO_2^+ UVD emission contain important information on the structure and dynamics of the Martian upper atmosphere. For instance, Cox et al. (2010) predicted an increase in the emission peak altitude from northern summer to northern winter, which they interpreted as a consequence of the thermospheric CO_2 density variation driven by global circulation. On the basis of the observed scale heights of the topside brightness profiles, Leblanc et al. (2006) derived an average temperature of 191 K at 130–170 km in the Martian thermosphere, and Bougher et al. (2017) further reported the seasonal and solar cycle variations in thermospheric temperature. Lo et al. (2015) estimated the CO_2 density structure from the CO_2^+ UVD observations, revealing clear tidal structures between 100 and 190 km. Finally, the Martian thermospheric response to solar flares was recently reported by Jain et al. (2018) based on the short-term variation in the same emission feature. Combining the IUVS observations and those made by other instruments on board MAVEN, such as the Neutral Gas and Ion Mass Spectrometer, would better elucidate the role of atmospheric variability in controlling CO_2^+ UVD emission, which we leave for follow-up studies.

5. Conclusions

Airglow emission provides important information on the structural variability of a planetary upper atmosphere under both external and internal drivers (Slanger et al., 2008, and references therein). This study is dedicated to a systematic investigation of the solar cycle and SZA variations in CO_2^+ UVD emission at Mars, a distinctive feature in a typical Martian dayglow spectrum that has been extensively studied over the past several decades (e.g., Barth et al., 1969, 1971; Stewart, 1972; Stewart et al., 1972; Leblanc et al., 2006; Cox et al., 2010; Jain et al., 2015, 2018; Gérard et al., 2019). Existing studies have established that this emission feature is mainly produced via photoionization and photoelectron impact ionization of atmospheric CO_2 (e.g., Fox and Dalgarno, 1979). For the purpose of this study, we analyzed a large number of CO_2^+ UVD brightness profiles collected by the MAVEN IUVS instrument when operated in the limb scan mode (McClintock et al., 2015), from which the respective peak emission intensities and altitudes were derived.

The available data set suggests the presence of strong solar cycle and SZA variations in both parameters, which manifest as (1) a significant increase in both peak intensity and altitude with increasing solar activity, and (2) a decrease in peak intensity but an increase in peak altitude with increasing SZA. Our analysis generally confirms previous results obtained either from the MEx SPICAM observations (e.g., Leblanc et al., 2006) or from a smaller set of the MAVEN IUVS observations available at an earlier epoch (e.g., Jain et al., 2015).

The observed solar cycle and SZA variations can be favorably interpreted by the solar-driven scenario in that (1) enhanced solar activity leads to enhanced production of excited-state CO_2^+ via photoionization and photoelectron impact ionization, as well as an expansion of the Martian upper atmosphere via solar heating; and (2) regions at a larger SZA feel a lower solar irradiance along a more slanted line of sight, which not only reduces the production of excited-state CO_2^+ but also elevates the location of unit optical depth. However, we note from the available IUVS observations that the solar-driven scenario is not able to account for all the details and an extra source of variability is required, presumably related to the complicated variations in the background atmosphere driven by global circulation, wave activity, and global dust storms, among others.

Acknowledgments

This work is supported by the B-type Strategic Priority Program (no. XDB41000000) funded by the Chinese Academy of Sciences and the pre-research project on Civil Aerospace Technologies (no. D020105) funded by the China National Space Administration. The authors also acknowledge support from the National Science Foundation of China (NSFC) through grants 41525015 and 41774186. The data used in this work are publicly available at the MAVEN Science Data Center (http://lasp.colorado.edu/maven/sdc/public/).

References

Barth, C. A., Fastie, W. G., Hord, C. W., Pearce, J. B., Kelly, K. K., Stewart, A. I., Thomas, G. E., Anderson, G. P., and Raper, O. F. (1969). Mariner 6: Ultraviolet spectrum of Mars upper atmosphere. *Science*, *165*(3897), 1004–1005. https://doi.org/10.1126/science.165.3897.1004

Barth, C. A., Hord, C. W., Pearce, J. B., Kelly, K. K., Anderson, G. P., and Stewart, A. I. (1971). Mariner 6 and 7 ultraviolet spectrometer experiment: Upper atmosphere data. *J. Geophys. Res.*, *76*(10), 2213–2227. https://doi.org/10.1029/JA076i010p02213

Bougher, S. W., Bell, J. M., Murphy, J. R., Lopez-Valverde, M. A., and Withers, P. G. (2006). Polar warming in the Mars thermosphere: Seasonal variations owing to changing insolation and dust distributions. *Geophys. Res. Lett.*, *33*(2), L02203. https://doi.org/10.1029/2005GL024059

Bougher, S. W., McDunn, T. M., Zoldak, K. A., and Forbes, J. M. (2009). Solar cycle variability of Mars dayside exospheric temperatures: Model evaluation of underlying thermal balances. *Geophys. Res. Lett.*, *36*(5), L05201. https://doi.org/10.1029/2008GL036376

Bougher, S. W., Roeten, K. J., Olsen, K., Mahaffy, P. R., Benna, M., Elrod, M., Jain, S. K., Schneider, N. M., Deighan, J., … Jakosky, B. M. (2017). The structure and variability of Mars dayside thermosphere from MAVEN NGIMS and IUVS measurements: Seasonal and solar activity trends in scale heights and temperatures. *J. Geophys. Res.*: *Space Phys.*, *122*(1), 1296–1313. https://doi.org/10.1002/2016JA023454

Cox, C., Gérard, J. C., Hubert, B., Bertaux, J. L., and Bougher, S. W. (2010). Mars ultraviolet dayglow variability: SPICAM observations and comparison with airglow model. *J. Geophys. Res.*: *Planets*, *115*(E4), E04010. https://doi.org/10.1029/2009JE003504

England, S. L., Liu, G., Yiğit, E., Mahaffy, P. R., Elrod, M., Benna, M., Nakagawa, H., Terada, N., and Jakosky, B. (2017). MAVEN NGIMS observations of atmospheric gravity waves in the Martian thermosphere. *J. Geophys. Res.*: *Space Phys.*, *122*(2), 2310–2335. https://doi.org/10.1002/2016JA023475

Eparvier, F. G., Chamberlin, P. C., Woods, T. N., and Thiemann, E. B. M. (2015). The solar extreme ultraviolet monitor for MAVEN. *Space Sci. Rev.*, *195*(1-4), 293–301. https://doi.org/10.1007/s11214-015-0195-2

Fox, J. L., and Dalgarno, A. (1979). Ionization, luminosity, and heating of the upper atmosphere of Mars. *J. Geophys. Res.*: *Space Phys.*, *84*(A12), 7315–7333. https://doi.org/10.1029/ja084ia12p07315

Fox, J. L. (1992). Airglow and aurora in the atmospheres of Venus and Mars. In J. G. Luhmann, et al. (Eds.), *Venus and Mars*: *Atmospheres, Ionospheres*, *and Solar Wind Interactions* (pp. 191-222). Washington: AGU. https://doi.org/10.1029/GM066p0191

Fox, J. L., and Yeager, K. E. (2009). MGS electron density profiles: Analysis of the peak magnitudes. *Icarus*, *200*(2), 468–479. https://doi.org/10.1016/j.icarus.2008.12.002

Fox, J. L., and Weber, A. J. (2012). MGS electron density profiles: analysis and modeling of peak altitudes. *Icarus*, *221*(2), 1002–1019. https://doi.org/10.1016/j.icarus.2012.10.002

Fu, M. H., Cui, J., Wu, X. S., Wu, Z. P., and Li, J. (2020). The variations of the Martian exobase altitude. *Earth Planet. Phys.*, *4*(1), 4–10. https://doi.org/10.26464/epp2020010

Gérard, J. C., Gkouvelis, L., Ritter, B., Hubert, B., Jain, S. K., and Schneider, N. M. (2019). MAVEN-IUVS observations of the CO_2^+ UV doublet and CO Cameron bands in the Martian thermosphere: Aeronomy, seasonal, and latitudinal distribution. *J. Geophys. Res.*: *Space Phys.*, *124*(7), 5816–5827. https://doi.org/10.1029/2019JA026596

Gkouvelis, L., Gérard, J. C., Ritter, B., Hubert, B., Schneider, N. M., and Jain, S. K. (2018). The O(^{1}S) 297.2-nm dayglow emission: A tracer of CO_2 density variations in the Martian lower thermosphere. *J. Geophys. Res.*: *Planets*, *123*(12), 3119–3132. https://doi.org/10.1029/2018JE005709

González-Galindo, Chaufray, F., Forget, J.-Y., García-Comas, F., Montmessin, M., F., Jain, S. K., &Stiepen, A. (2018). UV dayglow variability on Mars: Simulation with a global climate model and comparison with SPICAM/ MEx data. *Journal of Geophysical Research*: *Planets*, *123*, 1934–1952. https://doi.org/10.1029/2018JE005556

Jain, S. K., Stewart, A. I. F., Schneider, N. M., Deighan, J., Stiepen, A., Evans, J. S., Stevens, M. H., Chaffin, M. S., Crismani, M., … Jakosky, B. M. (2015). The structure and variability of Mars upper atmosphere as seen in MAVEN/IUVS dayglow observations. *Geophys. Res. Lett.*, *42*(21), 9023–9030. https://doi.org/10.1002/2015GL065419

Jain, S. K., Deighan, J., Schneider, N. M., Stewart, A. I. F., Evans, J. S., Thiemann, E. M. B., Chaffin, M. S., Crismani, M., Stevens, M. H., … Jakosky, B. M. (2018). Martian thermospheric response to an X8.2 solar flare on 10 September 2017 as seen by MAVEN/IUVS. *Geophys. Res. Lett.*, *45*(15), 7312–7319. https://doi.org/10.1029/2018GL077731

Jakosky, B. M., Lin, R. P., Grebowsky, J. M., Luhmann, J. G., Mitchell, D. F., Beutelschies, G., Priser, T., Acuna, M., Andersson, L., … Zurek, R. (2015). The Mars atmosphere and volatile evolution (MAVEN) mission. *Space Sci. Rev.*, *195*(1–4), 3–48. https://doi.org/10.1007/s11214-015-0139-x

Kass, D. M., Kleinböhl, A., McCleese, D. J., Schofield, J. T., and Smith, M. D. (2016). Interannual similarity in the Martian atmosphere during the dust storm season. *Geophys. Res. Lett.*, *43*(12), 6111–6118. https://doi.org/10.1002/2016GL068978

Leblanc, F., Chaufray, J. Y., Lilensten, J., Witasse, O., and Bertaux, J. L. (2006). Martian dayglow as seen by the SPICAM UV spectrograph on Mars Express. *J. Geophys. Res.*: *Planets*, *111*(E9), E09S11. https://doi.org/10.1029/2005JE002664

Lo, D. Y., Yelle, R. V., Schneider, N. M., Jain, S. K., Stewart, A. I. F., England, S. L., Deighan, J. I., Stiepen, A., Evans, J. S., … Jakosky, B. M. (2015). Nonmigrating tides in the Martian atmosphere as observed by maven IUVS. *Geophys. Res. Lett.*, *42*(21), 9057–9063. https://doi.org/10.1002/2015GL066268

McClintock, W. E., Schneider, N. M., Holsclaw, G. M., Clarke, J. T., Hoskins, A. C., Stewart, I., Montmessin, F., Yelle, R. V., and Deighan, J. (2015). The Imaging Ultraviolet Spectrograph (IUVS) for the MAVEN mission. *Space Sci. Rev.*, *195*(1-4), 75–124. https://doi.org/10.1007/s11214-014-0098-7

Morgan, D. D., Gurnett, D. A., Kirchner, D. L., Fox, J. L., Nielsen, E., and Plaut, J. J. (2008). Variation of the Martian ionospheric electron density from Mars Express radar soundings. *J. Geophys. Res.*: *Space Phys.*, *113*(A9), A09303. https://doi.org/10.1029/2008JA013313

Siddle, A. G., Mueller-Wodarg, I. C. F., Stone, S. W., and Yelle, R. V. (2019). Global characteristics of gravity waves in the upper atmosphere of Mars as measured by MAVEN/NGIMS. *Icarus*, *333*, 12–21. https://doi.org/10.1016/j.icarus.2019.05.021

Slanger, T. G., Cravens, T. E., Crovisier, J., Miller, S., and Strobel, D. F. (2008). Photoemission phenomena in the solar system. *Space Sci. Rev.*, *139*(1-4), 267–310. https://doi.org/10.1007/s11214-008-9387-3

Stevens, M. H., Evans, J. S., Schneider, N. M., Stewart, A. I. F., Deighan, J., Jain, S. K., Crismani, M., Stiepen, A., Chaffin, M. S., … Jakosky, B. M. (2015). New observations of molecular nitrogen in the Martian upper atmosphere by IUVS on MAVEN. *Geophys. Res. Lett.*, *42*(21), 9050–9056. https://doi.org/10.1002/2015GL065319

Stevens, M. H., Siskind, D. E., Evans, J. S., Fox, J. L., Deighan, J., Jain, S. K., and Schneider, N. M. (2019). Detection of the nitric oxide dayglow on Mars by MAVEN/IUVS. *J. Geophys. Res.*: *Planets*, *124*(5), 1226–1237. https://doi.org/10.1029/2019JE005945

Stewart, A. I. (1972). Mariner 6 and 7 ultraviolet spectrometer experiment: Implications of CO_2^+, CO and O airglow. *J. Geophys. Res.*, *77*(1), 54–68. https://doi.org/10.1029/JA077i001p00054

Stewart, A. I., Barth, C. A., Hord, C. W., and Lane, A. L. (1972). Mariner 9 ultraviolet spectrometer experiment: Structure of Mars' upper atmosphere. *Icarus*, *17*(2), 469–474. https://doi.org/10.1016/0019-1035(72)90012-7

Strausberg, M. J., Wang, H. Q., Richardson, M. I., Ewald, S. P., and Toigo, A. D. (2005). Observations of the initiation and evolution of the 2001 Mars global dust storm. *J. Geophys. Res.*: *Planets*, *110*(E2), E02006. https://doi.org/10.1029/2004JE002361

Thiemann, E. M. B., Chamberlin, P. C., Eparvier, F. G., Templeman, B., Woods, T. N., Bougher, S. W., and Jakosky, B. M. (2017). The MAVEN EUVM model of solar spectral irradiance variability at Mars: Algorithms and results. *J. Geophys. Res.*: *Space Phys.*, *122*(3), 2748–2767. https://doi.org/10.1002/2016JA023512

Wu, Z. P., Li, T., Zhang, X., Li, J., and Cui, J. (2020). Dust tides and rapid meridional motions in the Martian atmosphere during major dust storms. *Nat. Commun.*, *11*, 614. https://doi.org/10.1038/s41467-020-14510-x

Yao, M. J., Cui, J., Wu, X. S., Huang, Y. Y., and Wang, W. R. (2019). Variability of the Martian ionosphere from the MAVEN radio occultation science experiment. *Earth Planet. Phys.*, *3*(4), 283–289. https://doi.org/10.26464/epp2019029